


Lipid nanoparticles for administration of poorly water soluble neuroactive drugs

Elisabetta Esposito¹  · Markus Drechsler² · Paolo Mariani³ · Federica Carducci³ · Michela Servadio⁴ · Francesca Melancia⁴ · Patrizia Ratano⁵ · Patrizia Campolongo⁵ · Viviana Trezza⁴ · Rita Cortesi¹ · Claudio Nastruzzi¹

© Springer Science+Business Media New York 2017

Abstract This study describes the potential of solid lipid nanoparticles and nanostructured lipid carriers as nanoformulations to administer to the central nervous system poorly water soluble drugs. Different neuroactive drugs, i.e. dimethylfumarate, retinyl palmitate, progesterone and the endocannabinoid hydrolysis inhibitor URB597 have been studied. Lipid nanoparticles constituted of tristearin or tristearin in association with glyceryl monoolein were produced. The nanoencapsulation strategy allowed to obtain biocompatible and non-toxic vehicles, able to increase the solubility of the considered neuroactive drugs. To improve URB597 targeting to the brain, stealth nanoparticles were produced modifying the SLN surface with polysorbate 80. A behavioural study was conducted in rats to test the ability of SLN containing URB597 given by intranasal administration to alter behaviours relevant to psychiatric disorders. URB597 maintained its activity after nanoencapsulation, suggesting the possibility to propose

this kind of vehicle as alternative to unphysiological mixtures usually employed for animal and clinical studies.

Keywords Solid lipid nanoparticles · Nanostructured lipid carriers · Cryo-TEM · URB597 · Behaviour

Abbreviations

CNS	Central nervous system
SLN	solid lipid nanoparticles
NLC	nanostructured lipid carriers
DMF	dimethyl fumarate
RP	retinyl palmitate
PRG	progesterone
P80	polysorbate 80
cryo-TEM	cryogenic transmission electron microscopy
PCS	photon correlation spectroscopy
EE	encapsulation efficiency
LC	loading capacity
PTSD	post-traumatic stress disorder

Electronic supplementary material The online version of this article (doi:10.1007/s10544-017-0188-x) contains supplementary material, which is available to authorized users.

✉ Elisabetta Esposito
ese@unife.it

- ¹ Department of Life Sciences and Biotechnology, University of Ferrara, Via Fossato di Mortara, 19, I-44121 Ferrara, Italy
- ² BIMF/ Soft Matter Electronmicroscopy, University of Bayreuth, Bayreuth, Germany
- ³ Department of Life and Environmental Sciences and CNISM, Università Politecnica delle Marche, I-60100 Ancona, Italy
- ⁴ Department of Science, Roma Tre University, 00146 Rome, Italy
- ⁵ Department of Physiology and Pharmacology, Sapienza University of Rome, 00185 Rome, Italy

1 Introduction

It is well known that many neuroactive drugs are sparingly to practically insoluble in water, with about 90% of molecules in the discovery pipe-line being insoluble drugs (Kawabata et al. 2011). In particular, most drugs currently used for brain disorders are lipid-soluble (Banks 2009). Low solubility of drugs is a critical issue in preclinical and clinical research, since it often results in low bioavailability and limits therapeutic potential. At this regard, different strategies have been developed to increase drug solubility, spanning from the use of co-solvents or salt/pro-drug formation to the use of particle size reduction approaches (Shah et al. 2013; Merisko-Liversidge

and Liversidge 2011). In the case of neuroactive drugs, preclinical studies are often performed by dissolving drugs in non-aqueous solvents or unstable suspensions. In order to find alternative vehicles for insoluble molecules with central action, in the present study we propose the use of lipid nanoparticles. Lipid based nanoparticles have been recently proposed as biocompatible and biodegradable nanocarriers able to solubilize and deliver molecules with unfavorable physico-chemical properties controlling their release, to reduce drug dosage and number of administrations and to improve drug targeting/biodistribution (Mu et al. 2013; Vo et al. 2013). Different types of lipid nanoparticles can be distinguished as a function of the lipids constituting nanoparticle matrix, namely solid lipid nanoparticles (SLN) and nanostructured lipid carriers (NLC). Particularly, SLN are composed of lipids in solid state at room temperature, while NLC are constituted of solid and liquid lipid mixtures (Esposito et al. 2008; Esposito et al. 2015; Joshi and Müller 2009). In this context, the first part of the present study is focused on the production and characterization of SLN and NLC as vehicles for four neuroactive drugs characterized by poor water solubility and effective, either at the clinical or preclinical level, in the treatment of different CNS disorders: (1) dimethyl fumarate (DMF), that has proven useful in relapsing remitting multiple sclerosis, early brain injury and learning deficits (Bomprezzi 2015; Linker and Gold 2013); (2) retinyl palmitate (RP), whose supplementation can be considered as a new approach in multiple sclerosis prevention and treatment (Saboor-Yaraghi et al. 2015; Maden 2007); (3) progesterone (PRG), a neurosteroid that exerts neuroprotective effects in experimental brain insults, such as traumatic brain injuries (Webster et al. 2015) and (4) URB597, that increases endocannabinoid signaling by inhibiting the hydrolysis of the endocannabinoid anandamide and has significant anxiolytic-like, antidepressant-like, analgesic, cognitive, and prosocial effects in laboratory animals (Piomelli et al. 2006; Servadio et al. 2016; Morena et al. 2014; Morena et al. 2015).

In the second part of the study, we tested the effectiveness of lipid nanoparticles as alternative vehicle for neuroactive drugs. To this aim, we first increased the suitability of SLN to deliver URB597 to the brain, by treating SLN with polysorbate 80 (P80) to modify the nanoparticle surface. Indeed, a proper modification of SLN surface has been reported as highly effective strategy to alter SLN biodistribution, enhancing blood circulation time and deposition in non-RES organs (Göppert and Müller 2005; Ambruosi et al. 2005). Finally, since it has been shown that URB597, dissolved in organic solvents, has prosocial effects in laboratory animals (Manduca et al. 2014; Trezza et al. 2012), we tested the potential of SLN containing URB597 to alter brain function and behaviour, by testing their ability to modulate social behaviour in rats.

2 Materials and methods

2.1 Materials

The copolymer poly (ethylene oxide) (a) –poly (propylene oxide) (b) (a = 80, b = 27) (poloxamer 188) was a gift of BASF ChemTrade GmbH (Burgbernheim, Germany). Miglyol 812 N, caprylic/capric triglycerides (miglyol) was a gift of Cremer Oleo Division (Witten, Germany). Tristearin, stearic triglyceride (tristearin), polyoxyethylenesorbitan monooleate, polysorbate 80 (P80), dimethyl fumarate (DMF), retinyl palmitate (RP), progesterone (PRG) and URB597, [3-(3-carbamoylphenyl)phenyl] N-cyclohexylcarbamate (URB597) were purchased from Sigma-Aldrich, Merck (Darmstadt, Germany).

2.2 Determination of drug solubility

Solubility of drugs (see Table 1 for physico-chemical properties) in water, ethanol, water/ethanol, P80/ethanol and PEG400/P80/saline was determined by saturating each solvent or solvent mixture with an excess of drug. The obtained saturated solutions were moved overnight in a horizontal shaker (100 rpm; 37 ± 0.5 °C). At the end of the experiment 1 ml of samples were withdrawn and filtered through a Millex-LCR Filter, 0.45 µm, Hydrophilic PTFE, 25 mm (Millipore-Sigma-Aldrich Merck, Darmstadt, Germany). Concentration of drugs was determined by RP-HPLC analysis.

HPLC analysis was carried out by an Agilent Zorbax Eclipse XBD-C18 column (Agilent Technologies, United States) (15 cm × 0.46 cm) stainless steel packed with 5 µm particles, eluted at room temperature with different mobile phases. Samples of 50 µl were injected through the rheodyne injector system fitted with 50 µl fixed loop and compared with standards of known concentration. The mobile phase flow rate was 1 ml/min and the composition was: acetonitrile/water (25:75, v/v), methanol/water (70:30, v/v), methanol and methanol/water (80:20, v/v), for DMF, RP, PRG and URB597 respectively. Chromatograms were obtained with a UV detector set at 220 nm for DMF, 350 nm for RP, 254 nm for PRG and 280 nm for URB597. Analyses were conducted in triplicate, mean and standard deviations values were calculated.

2.3 Preparation of lipid nanoparticles

Lipid nanoparticles were prepared by melt and ultrasonication, following a previously reported method with minor modifications (Esposito et al. 2016). The lipid phase (5% with respect to the whole weight of the dispersion) was constituted of pure tristearin (in

Table 1 Characteristics and uses of the drugs employed in the present study

Drugs	Molecular weight (g/mol)	Melting point (°C)	log P	pKa	use
Dimethyl fumarate (DMF)	144.13	104	0.72	-6.5 ^a	psoriasis; multiple sclerosis; early brain injury
Retinyl palmitate (RP)	524.86	28	11.62	-7	antioxidant; regeneration and maintenance of the nervous system
Progesterone (PRG)	314.46	128	3.87	18.92	pregnancy maintenance; traumatic brain injury treatment
URB597	338.40	121	4.03	11.74 ^b	inflammatory pain states; post-traumatic stress disorders; psychopathological disorders associated with social dysfunctions, i.e. autism and schizophrenia

^a strongest basic

^b acidic pKa determined by ACD

the case of SLN preparation) or a mixture of tristearin and miglyol in a 2:1 w/w ratio (in the case of NLC preparation). Briefly, an aqueous poloxamer 188 solution (2.5% w/w) heated at 80 °C was added to the molten lipid phase, afterwards the mixture was emulsified at 15000 rpm, 80 °C for 1 min, subjected to ultrasonication at 6.75 kHz for 15 min and then let cooling at 25 °C. Lipid nanoparticle dispersions were stored at room temperature. In the case of drug containing nanoparticles, the drug was added to the molten lipid phase before adding the aqueous poloxamer 188 solution. Table 2 reports the abbreviations used throughout the text to indicate the different nanoparticles and their compositions.

2.4 Modification of SLN surface with polysorbate 80

For the preparation of modified nanoparticle, namely: SLN/P80 and SLN/P80-URB597, P80 (20% w/w with respect to the lipid weight) was added to the SLN dispersion during the preparation, specifically after the ultrasonication step, when the dispersion was at 40 °C; stirring at 250 rpm was maintained until the preparation was cooled down at room temperature (typically in 30 min).

Table 2 Solubility of the drugs employed in the present study

Solvents		Drug solubility (mg/ml)			
		Dimethyl fumarate (DMF)	Retinyl palmitate (RP)	Progesterone (PRG)	URB597
Water		1.58 ± 0.01	0.007 ± 0.0	0.009 ± 0.00	0.01 ± 0.00
Ethanol/water (v/v)	50:50	n.d.	n.d.	0.67 ± 0.02	0.1 ± 0.01
	20:80	0.14 ± 0.01	0.14 ± 0.01	0.1 ± 0.01	0.05 ± 0.00
	10:90	0.54 ± 0.01	0.54 ± 0.01	0.03 ± 0.01	0.03 ± 0.00
Ethanol		16.22 ± 0.2	1.09 ± 0.03	1.00 ± 0.01	4.60 ± 0.02
Ethanol/P80* (v/v)	10:90	0.72 ± 0.02	0.72 ± 0.02	0.14 ± 0.01	0.04 ± 0.00
	20:80	0.18 ± 0.01	0.18 ± 0.01	0.21 ± 0.01	0.03 ± 0.00

*Aqueous solution of polysorbate 80 1% w/w

2.5 Cryogenic transmission electron microscopy (cryo-TEM) analysis

Samples were vitrified as previously described (Esposito et al. 2012). The vitrified specimen was transferred to a Zeiss EM922Omega transmission electron microscope for imaging using a cryoholder (CT3500, Gatan). The temperature of the sample was kept below -175 °C throughout the examination. Specimens were examined with doses of about 1000–2000 e/nm² at 200 kV. Images were recorded digitally by a CCD camera (Ultrascan 1000, Gatan) using an image processing system (GMS 1.9 software, Gatan). In addition, size distribution of nanoparticles was performed by measuring 1000 nanoparticles for each cryo-TEM image by the digital analyzer ImageJ 1.48v.

2.6 Photon correlation spectroscopy (PCS) analysis

Submicron particle size analysis was performed using a Zetasizer 3000 PCS (Malvern Instr., Malvern, England) equipped with a 5-mW helium neon laser with a wavelength output of 633 nm. Glassware was cleaned of dust by washing with detergent and rinsing twice with water for injections. Measurements were made at 25 °C at an

angle of 90°. Data were interpreted using the “CONTIN” method (Pecora 2000).

2.7 X-ray diffraction measurements

X-ray diffraction experiments were performed using a 3.5 kW Philips PW 1830 X-ray generator (Amsterdam, Netherlands) equipped with a Guinier-type focusing camera (homemade design and construction, Ancona, Italy) operating with a bent quartz crystal monochromator ($\lambda = 1.54 \text{ \AA}$). Diffraction patterns were recorded on GNR Analytical Instruments Imaging Plate system (Novara, Italy). Samples were held in a tight vacuum cylindrical cell provided with thin mylar windows. Diffraction data were collected at 37°. In each experiment, Bragg peaks were detected. The few peaks in the low-angle region were indexed considering the different symmetries commonly observed in lipidic phases (Luzzati et al. 1997) and the unit cell dimension of the phase, a , calculated from the averaged spacing of the observed peaks. Peaks in the wide-angle x-ray scattering region relate to the lateral organization of the hydrocarbon chains: from their positions, the subcell structure of the nanoparticles was determined.

2.8 Encapsulation efficiency and loading capacity of lipid nanoparticles

Determinations were performed six times in independent experiments and the mean values \pm standard deviations were calculated.

The encapsulation efficiency (EE) and loading capacity (LC) of DMF, RP, PRG and URB597 in SLN and NLC were determined as previously described (Esposito et al. 2015). 100 μl aliquot of each SLN and NLC batch was loaded in a centrifugal filter (Microcon centrifugal filter unit YM-10 membrane, NMWCO 10 kDa, Sigma Aldrich, St Louis, MO, USA) and centrifuged (Spectrafuge™ 24D Digital Microcentrifuge, Woodbridge NJ, USA) at 8000 rpm for 20 min. The amount of drug was determined after dissolving the lipid phase with a known amount of methanol (1:10, v/v) by high performance liquid chromatography (HPLC), as above reported. EE and LC were determined following eqs. (1) and (2), respectively.

$$EE = L/T \times 100 \quad (1)$$

$$LC = L/T_{\text{lipid phase}} \times 100 \quad (2)$$

where L is the amount of drug loaded in SLN or in NLC, T stands for the total amount of drug added to the formulation and $T_{\text{lipid phase}}$ for the total weight of lipid phase in the formulation. Determinations were performed six times in independent experiments and the mean values \pm standard deviations were calculated.

2.9 *In vitro* URB597 release studies

In vitro dialysis release studies were performed on URB597 alternatively solubilized in PEG 400/P80/saline 5:5:90 (v/v/v), in SLN/P80, or suspended in poloxamer 188 solution (2.5% w/w). Two milliliters of solution/suspension (URB597 0.2 mg/ml) were placed into a dialysis tube (6 cm) (molecular weight cut off 10,000–12,000; Medi Cell International, England), then placed into 30 ml of receiving phase constituted of phosphate buffer (100 mM, pH 7.4) and ethanol (70:30, v/v) and shaken in a horizontal shaker (MS1, Minishaker, IKA) at 175 rpm at 37 °C. Samples of receiving phase were withdrawn at regular time intervals, and analyzed by HPLC method as described below. Fresh receiving mixture was added to maintain constant volume. The URB597 concentrations were determined six times in independent experiments and the mean values \pm standard deviations were calculated.

2.10 Drug release data analysis

The experimental release data obtained by the release experiments were fitted to the following semi-empirical equations respectively describing Fickian dissolutive (3) and diffusion (4) release mechanisms (Peppas 1985; Siepmann and Siepmann 2008)

$$Mt/M_{\infty} = K_{\text{Diss}} t^{0.5} + c \quad (3)$$

$$1 - Mt/M_{\infty} = e^{-K_{\text{diff}} t} + c \quad (4)$$

where Mt / M_{∞} is the drug fraction released at the time t , (M_{∞} is the total drug content of the analyzed amount of SLN), K and c are coefficients calculated by plotting the linear forms of the indicated equations. The release data of percentage of released drug (0–8 h) were used to produce theoretical release curves.

2.11 *In vivo* behavioural evaluation

Male adolescent Wistar Han rats (28–35 g at the time of the experiments; Charles River Laboratories, France) were housed in groups of six in a temperature-controlled ($20 \pm 1 \text{ }^{\circ}\text{C}$) vivarium and maintained under a 12 h light/dark cycle (07:00 AM–07:00 PM h lights on). Food and water were available ad libitum. The experiments were approved by the Italian Ministry of Health (Rome, Italy) and performed in agreement with the guidelines released by the Italian Ministry of Health (D.L. 26/14) and the European Community Directive 2010/63/EU.

Social behaviour was assessed as previously described (Manduca et al. 2014; Trezza and Vanderschuren 2008a; Trezza and Vanderschuren 2008b). The experiments were performed in a sound attenuated chamber. The testing arena consisted of a Plexiglas cage measuring $45 \times 45 \times 60 \text{ cm}$ (l

x w x h), with approximately 2 cm of wood shavings covering the floor.

The animals were individually habituated to the test cage for 10 min on each of the two days prior to testing. On the testing day, the animals were socially isolated for 3 h before the test. Two hours before testing, pairs of animals were treated by intranasal route with either SLN/P80-URB597 or SLN/P80 at the dose of 0.1 mg/Kg. Drug dose and pre-treatment interval were based on literature. In preclinical studies, URB597 is usually dissolved in a mixture of plain PEG400/P80/saline and, administered by intraperitoneal (i.p.) injection 2 h before testing at the dose of 0.1 mg/kg, has prosocial effects in rats (Manduca et al. 2014; Trezza and Vanderschuren 2008a; Trezza and Vanderschuren 2008b). Therefore, as additional control, other pairs of rats were treated with URB597 (0.1 mg/kg, i.p.) dissolved in PEG400/P80/saline or plain PEG400/P80/saline.

The social behaviour test consisted of placing two similarly treated animals into the test cage for 15 min. The animals of each pair did not differ more than 10 g in body weight and had no previous common social experience (i.e., they were not cage mates). The behaviours of the animals were recorded using a camera with zoom lens, video tape recorder and television monitor. Behaviour was assessed per pair of animals and analyzed by a trained observer who was unaware of treatment condition using the Observer XT software (Noldus, Wageningen, The Netherlands).

In rats, a bout of social play behaviour starts with one rat soliciting ('pouncing') another animal, by attempting to nose or rub the nape of its neck. The animal that is pounced upon can respond in different ways: if the animal fully rotates to its dorsal surface, 'pinning' is the result (one animal lying with its dorsal surface on the floor with the other animal standing over it), which is considered the most characteristic posture on social play behaviour in rats (Pellis and Pellis 1987).

During the social encounter, animals may also display social behaviours not directly associated with play, such as sniffing or grooming the partner's body (Panksepp and Beatty 1980; Vanderschuren et al. 1995). In the present study, both animals in a play pair were similarly treated and a pair of rats was considered as one experimental unit.

The following parameters were therefore scored per pair of animals:

Social behaviours directly related to play:

- frequency of pinning
- frequency of pouncing

Social behaviours unrelated to play:

- time spent in social exploration: the total amount of time spent in non-playful forms of social interaction

(i.e., one animal sniffing or grooming any part of the partner's body).

2.12 Statistical analysis

In vivo data are expressed as mean \pm SEM. Data were analyzed using Student's t test. *P* values of less than 0.05 were considered statistically significant.

3 Results and discussion

3.1 Drug selection and solubility studies

Aim of this investigation is to design vehicles (based on nanoparticle) for a selection of neuroactive drugs, whose characteristics are reported in Table 1. Common feature of the selected drugs is the lipophilicity, reflected by the log *P* ranging between 0.72 and 11.62, being slightly soluble or practically insoluble in water. The two extremes are represented by DMF (log *P* 0.72; solubility 1.58 mg/ml) and RP (log *P* 11.62, solubility 7.00×10^{-3} mg/ml). The drugs have been chosen since they are effective, either at the clinical or preclinical level, in the treatment of different CNS disorders. Indeed, DMF and PRG are employed to treat brain injuries (e.g. early or traumatic respectively) (Liu et al. 2015; Webster et al. 2015); RP has been proposed as a new therapeutic tool for multiple sclerosis (Saboor-Yaraghi et al. 2015; Maden 2007); URB597 is effective in animal models of anxiety, depression, and autism spectrum disorders (Piomelli et al. 2006; Servadio et al. 2016).

Initially, the solubility of the molecules has been determined in water, ethanol and water/ethanol mixtures as reported in Table 2. In the case of all drugs the highest solubility was observed in pure ethanol.

Since different studies have demonstrated that ethanol induces acute intravenous toxicity in animals and behavioural effects in humans by inhalation (Montaguti and Melloni 1994; Cosmetic Ingredient Expert Review Panel 2008; Pastino et al. 1997), we chose to study alternative strategies to encapsulate the drugs. In particular, the possibility to encapsulate DMF, RP, PRG and URB597 in lipid nanoparticles was investigated.

3.2 Preparation and characterization of lipid nanoparticle

Both SLN and NLC have been prepared based on the composition reported in Table 3, following a method previously assessed by our group (Esposito et al. 2016). Notably SLN were constituted of pure tristearin, while to produce NLC a mixture of tristearin and miglyol was employed.

The effect of the drug presence in SLN and NLC has been investigated with respect to morphology, dimensions and encapsulation efficiency.

Table 3 Composition of SLN and NLC

Nanoparticle	Composition (% w/w)					
	tristearin	miglyol	poloxamer 188	water	polysorbate 80	drug
empty SLN	5.0	-	2.37	92.63	no	-
SLN/P80	5.0	-	2.37	92.63	yes	-
empty NLC	5.0	-	2.37	92.63	no	-
SLN-DMF	5.0	-	2.37	92.53	no	0.1
NLC-DMF	3.34	1.66	2.37	92.53	no	0.1
SLN-RP	5.0	-	2.37	92.59	no	0.04
NLC-RP	3.34	1.66	2.37	92.59	no	0.04
SLN-PRG	5.0	-	2.37	92.53	no	0.1
NLC-PRG	3.34	1.66	2.37	92.53	no	0.1
SLN-URB597	5.0	-	2.37	92.61	no	0.02
SLN/P80-URB597	5.0	-	2.37	92.61	yes	0.02
NLC-URB597	3.34	1.66	2.37	92.61	no	0.02

Particularly, cryo-TEM enabled a direct visualization of the morphology of the produced nanoparticles when dispersed in water. The microphotographs reported in Fig. 1 show the morphology of SLN (A-D) and NLC (E-H) containing different drugs, namely: DMF (A, E), RP (B, F), PRG (C, G) and URB597 (D, H).

For the analysis of the cryo-TEM images, it is important to underline that this technique results in the formation of many images in case of complex 3D structures having different orientations. Both SLN and NLC possess a general typical discoid morphology, appearing as relatively low electron density regions with a circular/elliptic shape (white arrows) when viewed from the top; or as electron-dense bars, when edge-on viewed. Regarding the effect of drug presence on the morphology of SLN and NLC, some indications can be raised; (i) no significant differences are appreciable between empty and drug loaded nanoparticles, (ii) DMF, PRG or URB597 nanoparticles are almost identical each other, indicating that the presence of these drugs does not affect the nanoparticle morphology, (iii) only in the case of NLC-RP nanoparticles the structure appears more evanescent, suggesting that the presence of RP could cause a disorganization of nanoparticle internal structure.

With respect to the internal structure (well appreciable in the edge-viewed nanoparticles), when imaged at higher magnification (see Fig. 2 and Table 4) some differences appear evident by the comparison of SLN with NLC.

In the case of SLN-DMF (Fig. 2a) and SLN-RP (Fig. 2b), edge-on nanoparticles appear as bilayered lamellar structures, resembling a bicellar organization, while in the case of SLN-PRG (Fig. 2c) and SLN-URB597 (Fig. 2d) they appear as flat discoids with electron dense surfaces. The images of NLC

(Figs. 2e-h) show a different shape, with the predominant presence of a multilamellar internal structure capped with semi-elliptical surfaces. The structure of NLC is well in agreement with that previously described by other authors, Jores and colleagues attributed this specific morphology to the presence of miglyol, which is liquid at room temperature, forming caps on the lamellar structure (Jores et al. 2004).

The dimensional data, obtained by PCS, reported in Table 4 by Z average or number, indicate that nanoparticles have diameters comprised between 129 and 254 nm and dispersity comprised between 0.24–0.3. No main differences were found between SLN and NLC diameter, in the absence or in the presence of drugs.

The analysis of the X-ray scattering low-angle region confirmed the lamellar morphology of nanoparticles. Particularly, Table 4 reports the interlamellar distances a of the different nanoparticle samples. Results indicate that NLC were characterized by slightly larger interlamellar distances with respect to the corresponding SLN. This finding suggests an expanded packing in the presence of miglyol.

3.3 Drug encapsulation in lipid nanoparticles

The ability of both SLN and NLC to solubilize by encapsulation the selected drugs was investigated. In this respect, the determined EE and LC values are reported in Table 4; notably the obtained EE data follow the decreasing order URB > DMF > PRG > RP. Apart from DMF which was more effectively encapsulated within SLN, for the other drugs EE values in SLN and NLC were similar. LC was in all cases low since the tested drugs are all extremely powerful and their dosage low, therefore the amount of drug used for the encapsulation was always below 20 $\mu\text{g}/\text{mg}$ (drug weight/total lipid weight).

Fig. 1 Cryo-TEM images of SLN (**a-d**) and NLC (**e-h**) containing different drugs, namely DMF (**a, e**), RP (**b, f**), PRG (**c, g**), URB597 (**d, h**). Bar corresponds to 100 nm. For nanoparticle acronym and composition please refer to experimental section

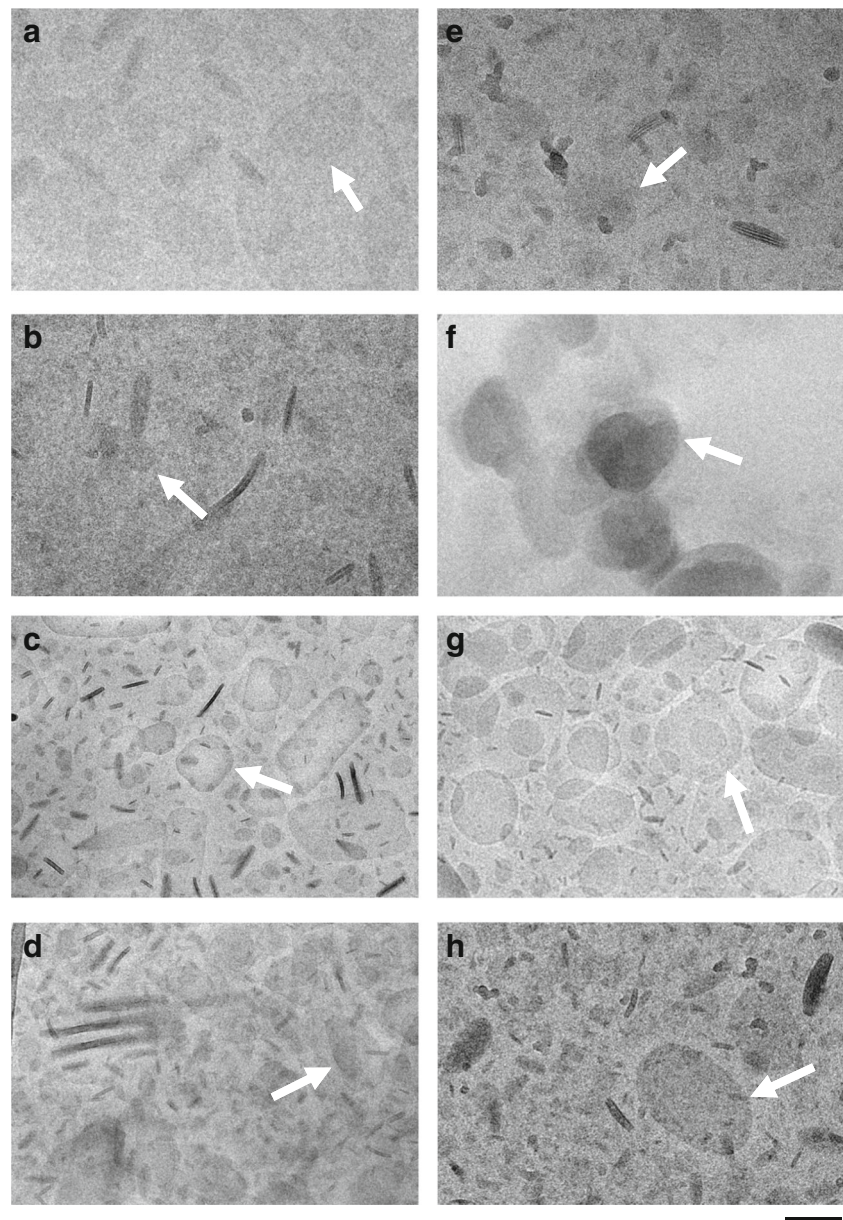


Fig. 3 reports the comparison of the drug solubility in SLN and NLC with that in PEG 400/P80/saline, representing a standard vehicle usually employed for clinical and preclinical studies (Morgese et al. 2009; Achterberg et al. 2014; Martínez et al. 2015). The results appear very impressive since lipid nanoparticles can improve the solubility of all tested drug with respect to PEG400/P80/saline. Particularly, for RP and PRG the improve in solubility was marked, indeed RP solubility passed from 0.17 to 1.35 and 1.45 mg/ml in SLN and NLC respectively, while PRG solubility increased from 0.69 to 2.9 and 2.95 mg/ml in SLN and NLC respectively.

In the case of URB597, the molecule displaying the lowest solubility in PEG 400/P80/saline (0.12 mg/ml),

the increase in solubility was less marked (about 1.5-fold), nevertheless since URB597 has an interesting pharmacological profile (i.e. to treat post-traumatic stress disorders), a further investigation of the potential of SLN as delivery system for URB597, was undertaken.

3.4 Modification of SLN surface with polysorbate 80

To ameliorate the brain targeting of SLN-URB597, the treatment of nanoparticles with polysorbate 80 was evaluated.

It is well known that P80 has a so-called “stealth effect” and it exerts a specific role in brain targeting (Göppert

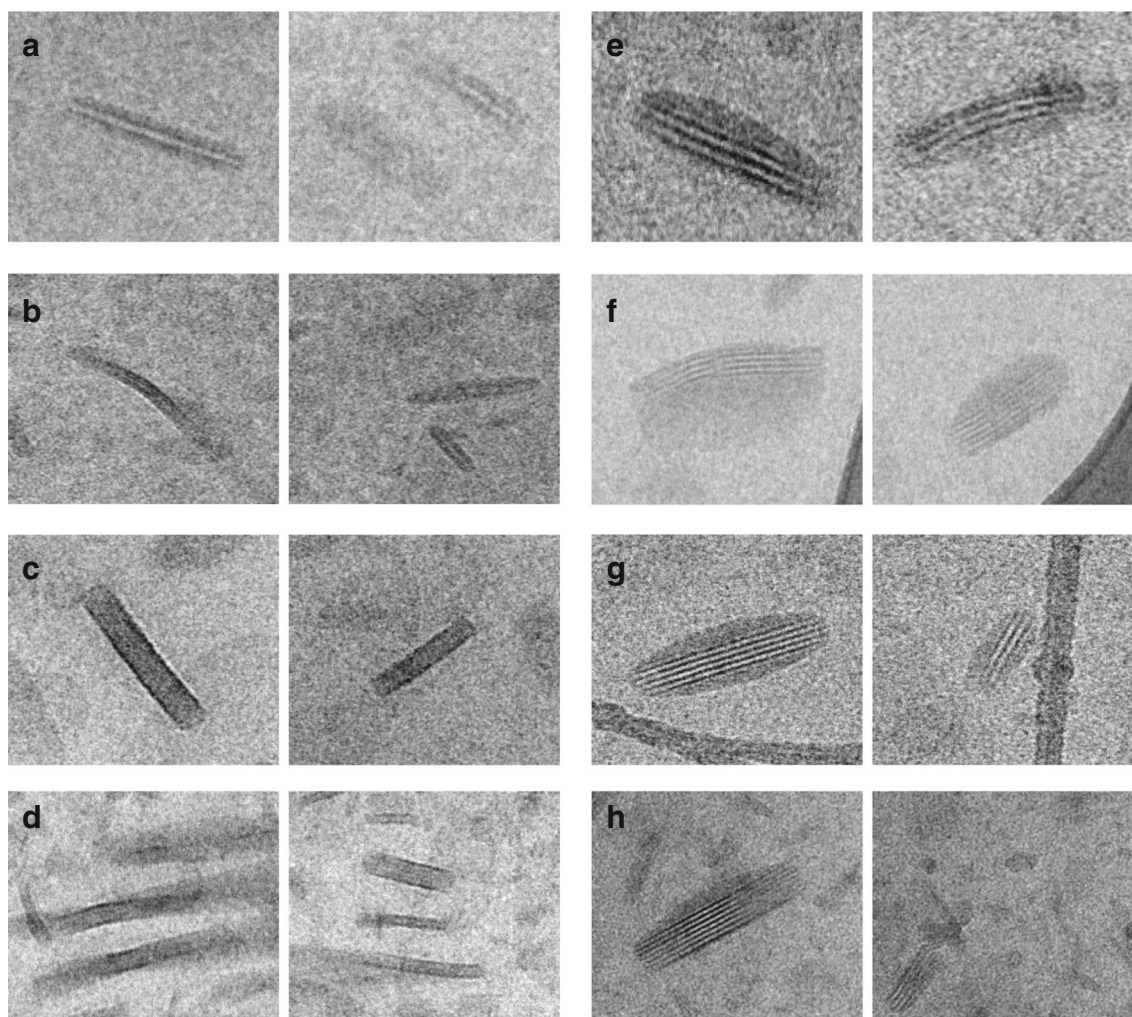


Fig. 2 Cryo-TEM edge-on-viewed images of SLN (**a-d**) and NLC (**e-h**) containing different drugs, namely DMF (**a, e**), RP (**b, f**), PRG (**c, g**), URB597 (**d, h**). Bar corresponds to 100 nm. For nanoparticle acronym and composition please refer to experimental section

and Müller 2005). Indeed, unmodified nanoparticles are mostly captured by opsonins and eliminated from the body by phagocyte cells (Ambrusi et al. 2005), whereas nanoparticles coated with polyethylene glycol (PEG) are scarcely captured by the RES and can circulate for long. Moreover, P80 is supposed to inhibit the transporter P-glycoprotein that exerts a role in the efflux of endogenous and exogenous compounds across biological membranes, such as the BBB (Amin 2013).

The treatment of SLN with P80 results in the penetration of P80 hydrophobic fatty acid chains within the lipid matrix not yet completely consolidated. Hence, the PEG chains (representing the hydrophilic portion of P80) protrude into the aqueous phase out from SLN surface, protecting the SLN from the environment, while the lipophilic portion of P80 acts as a lipid anchor.

Since PEGylation changes the physicochemical properties of nanoparticles, morphology, dimension and inner structure of SLN treated by P80, in the absence and in the presence of URB have been determined.

Fig. 4 shows a comparative analysis of cryo-TEM morphology of SLN produced in the absence (panels A and C) or in the presence of URB597 (panels B and D); specifically, control untreated SLN are reported in panels A and B, whereas those treated with P80 are reported in panels C and D. Untreated nanoparticles display a flat discoidal shape, whilst the presence of P80 causes a shift towards a bicellar like structure.

Regarding nanoparticle dimensions, the treatment with P80 led to a small increase (30–50 nm) of the mean diameter (Table 4).

URB597 containing nanoparticles were further characterized by low and wide angle X-ray scattering analysis.

Table 4 Dimensional characteristics, structural organization and encapsulation parameters of the indicated nanoparticles

Nanoparticle	Dimensional characteristics			X-ray diffraction interlamellar distance (nm)	Cryo-TEM morphology	EE ^a (%)	LC (%)
	Z average (nm)	Diameter by number (nm)	Dispersity				
empty SLN	147 ± 52	98 ± 23	0.26 ± 0.01	3.74	flat discoid	-	-
SLN/P80	176 ± 25	120 ± 13	0.25 ± 0.08	4.55	bicellar	-	-
empty NLC	179 ± 55	106 ± 20	0.27 ± 0.01	4.55	capped multilamellar	-	-
SLN-DMF	254 ± 28	110 ± 22	0.25 ± 0.01	3.81	bicellar	85.2	1.7
NLC-DMF	195 ± 20	99 ± 15	0.25 ± 0.01	4.49	capped multilamellar	71.2	1.4
SLN-RP	192 ± 46	105 ± 12	0.27 ± 0.04	4.60	bicellar	45.1	0.3
NLC-RP	129 ± 22	99 ± 15	0.24 ± 0.03	4.68	capped multilamellar	48.3	0.4
SLN-PRG	160 ± 70	104 ± 18	0.30 ± 0.02	3.80	flat discoid	72.5	1.4
NLC-PRG	187 ± 64	130 ± 28	0.29 ± 0.03	4.52	capped multilamellar	73.8	1.5
SLN-URB597	246 ± 33	122 ± 21	0.28 ± 0.03	4.50	flat discoid	93.0	0.4
SLN/P80-URB597	273 ± 20	122 ± 22	0.30 ± 0.03	4.48	bicellar	93.0	0.4
NLC-URB597	242 ± 45	104 ± 8	0.29 ± 0.01	4.69	capped multilamellar	92.8	0.4

Data are the means ± SD of 6 independent batches

^apercentage (w/w) of drug in the whole dispersion with respect to the total amount used for the preparation

Results reported in Fig. 5 can be summarized as follows. In low-angle analyses (Fig. 5 a, c, e), the observed Bragg peaks indicate a lamellar order in the investigated samples: however, the similar scattering profile detected in SLN and NLC suggests that the crystal lamellar packing order was scarcely affected by the presence of miglyol, as observed by other authors (Jenning et al. 2000). Notably, in the case of SLN/P80-URB597, a decrease in the diffraction peak intensity is detectable, indicating that P80 presence decreased the structural order organization of SLN (Fig. 5c).

Scattering profiles in the wide-angle region (Fig. 5 b, d, f) enabled to obtain information about the subcell crystalline nature of nanoparticles. The analyzed samples

displayed diffraction patterns characterized by the presence of different peaks, whose positions are reported in Table 5. Notably, both in the SLN and NLC data it is possible to observe a strong main peak at 0.46 nm (peak #1 in the Fig. 5) and two weak peaks at 0.37 and 0.39 nm (peak #2 and #3 in the same figure). Such profile is ascribable to a β inner organization, triclinic parallel. Interestingly, in the case of P80 nanoparticles, peaks #2 and #3 were not present, probably because P80 affected the nanoparticle structure or order.

3.5 *In vitro* release kinetics of URB597 from SLN

To investigate the performance of SLN/P80 as delivery systems for URB597 with respect to a solution of the drug in PEG 400/P80/saline and a suspension of the drug in poloxamer 188 (2.5% w/w) in water) taken as controls, the release profiles from SLN/P80-URB597 were determined *in vitro* by a dialysis method.

All release profiles, reported in Fig. 6, were characterized by an initial phase in which URB597 is almost linearly released up to 50–60%, followed by a slower phase, in which the remaining drug is released in about 5–6 h. The release kinetic of URB597 from SLN/P80 was almost superimposable to that from PEG 400/P80/saline, on the contrary, as expected, the release of URB597 in the suspension form was reduced, specifically in the slower phase.

Moreover, a mathematical analysis of the release profile of URB597 from SLN/P80-URB597 was conducted

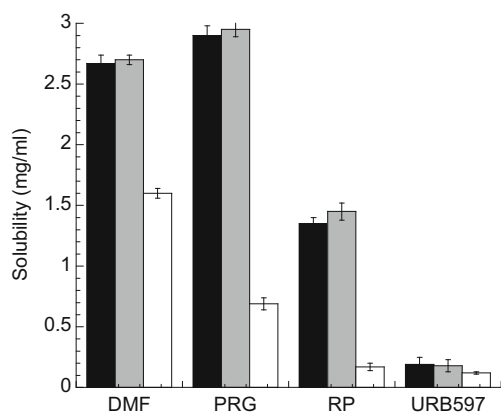


Fig. 3 Comparative analysis of drug solubility in SLN (black), NLC (grey) and PEG 400/P80/saline 5:5:90 (v/v/v) (white)

Fig. 4 Cryo-TEM images of SLN (a), SLN-URB597 (b), SLN/P80 (c) and SLN/P80-URB597 (d). Bar corresponds to 200 nm. For nanoparticle acronym and composition please refer to experimental section

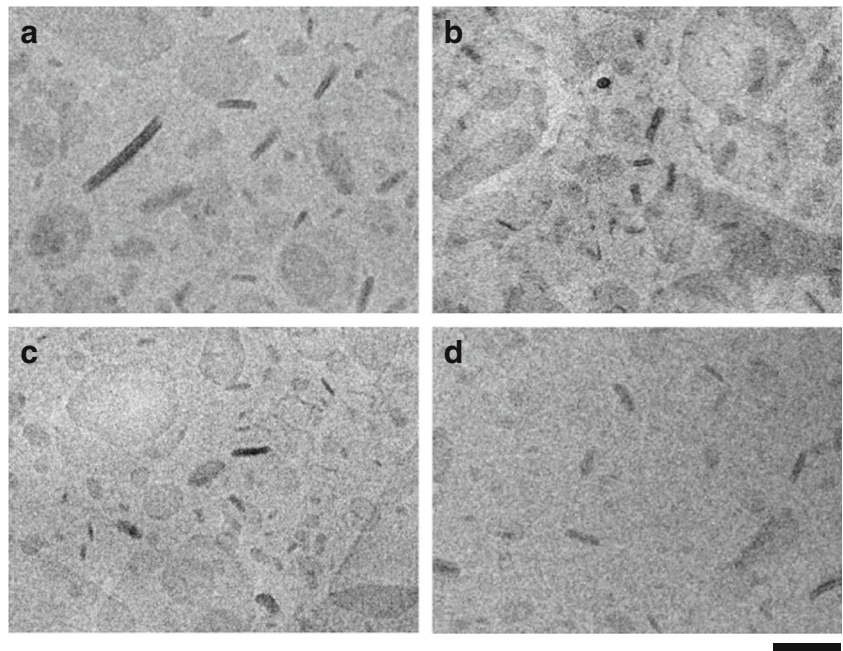


Fig. 5 Low (a-c-e) and wide-angle (b-d-f) X-ray diffraction profiles for the different nanoparticles measured at 25 °C. a and b: NLC-URB597 (upper profile) and SLN-URB597 (lower profile); c and d: two different batches of SLN-URB597; E and F: SLN/P80-URB597 (upper curve) and SLN-URB597 (lower curve)

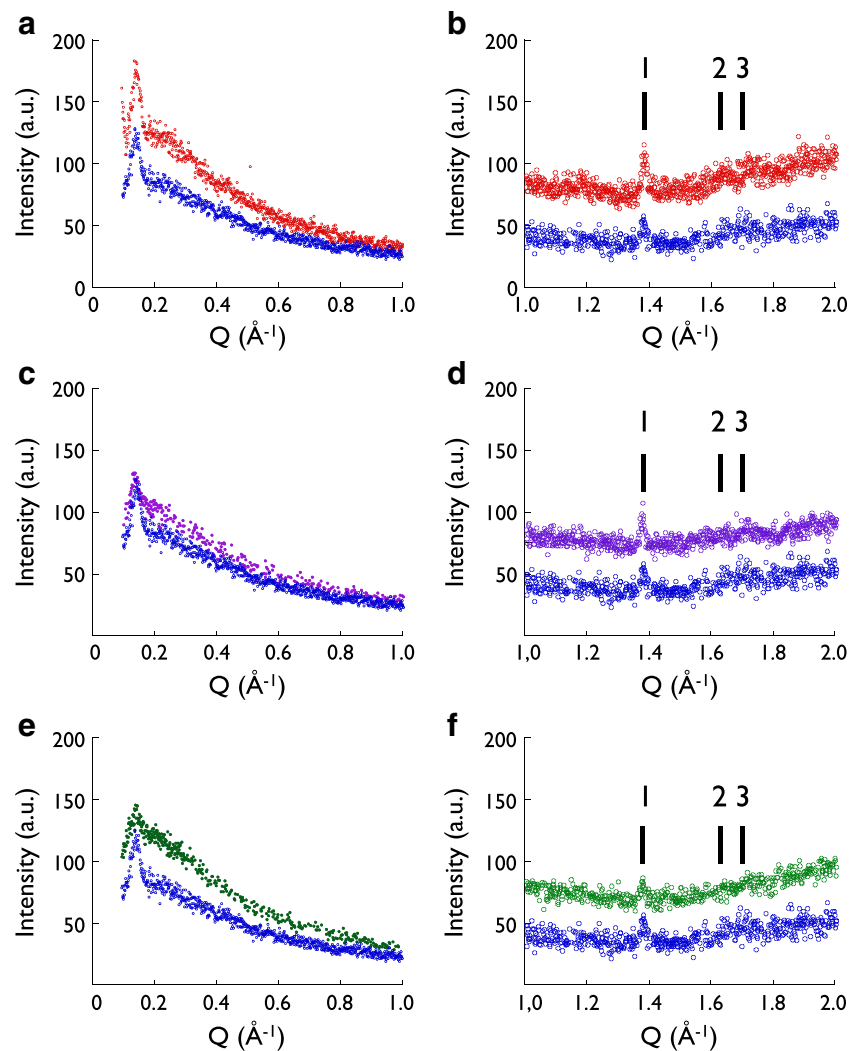


Table 5 Positions of the wide-angle X-ray diffraction peaks observed in the different nanoparticles

Peak positions			
Nanoparticle	Peak#	q (Å ⁻¹)	d (nm)
NLC-URB597	1	1.37	0.46
	2	1.63	0.39
	3	1.71	0.37
SLN -URB597	1	1.37	0.46
	2	1.63	0.39
	3	1.71	0.37
SLN/P80-URB597	1	1.37	0.46
	2	n.p.	n.p.
	3	n.p.	n.p.

n.p not present

to evaluate the mechanism of drug release. URB597 theoretical release profiles were determined according to the linear form of Eq. (3) mimicking a dissolutive model (Fig.7 a) and Eq. (4) mimicking a diffusive model (Fig.7 b). Thereafter, a comparison between the theoretical and experimental URB597 release from SLN/P80-URB597 was performed (Fig. 7 c).

From the analysis of the data, it is evident that the experimental curve is almost superimposable to the theoretical curve calculated from Eq. (3), suggesting a release more consistent with a dissolutive rather than diffusive process, as proven by the higher value of R found in the case of linearization of Eq. (3) (reported in Fig. 7 a); therefore, it can be concluded that the release of URB597 appears predominantly governed by a non-fickian dissolution mechanism (Siepmann and Siepmann 2008).

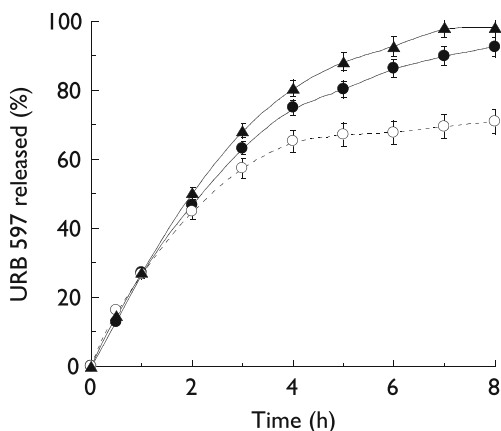


Fig. 6 *In vitro* release kinetics of URB597 from SLN/P80-URB597 (●), poloxamer 188 solution (2.5% w/w) (■) and PEG 400/P80/water 5:5:90 (v/v/v) (▲). Experiments were performed by dialysis method. Data are the mean of 6 experiments ± S.D. For nanoparticle acronym and composition please refer to experimental section

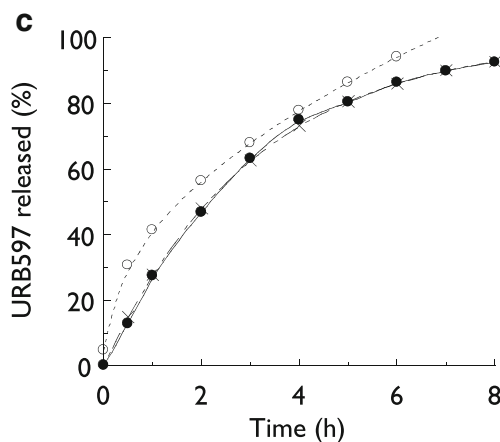
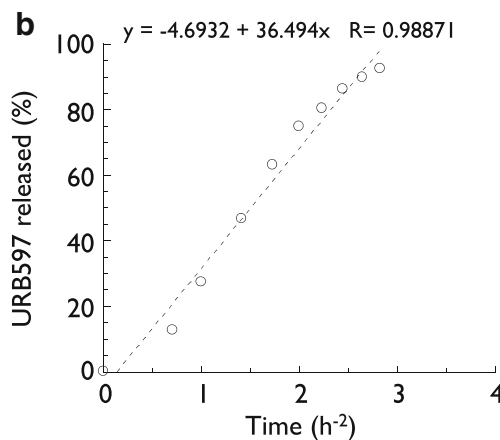
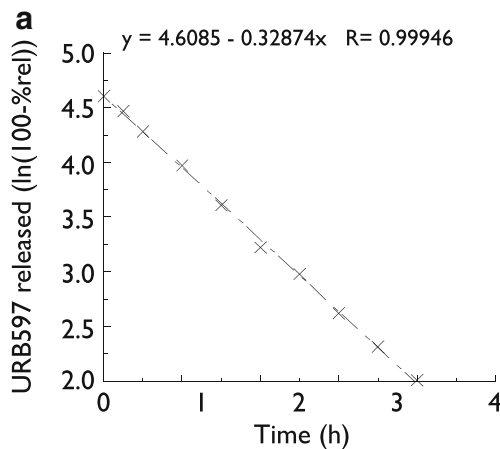


Fig. 7 Comparison of the theoretical (dotted lines) and experimental (solid lines) URB profiles from SLN/P80-URB597. The theoretical curves were obtained using the coefficient calculated by linear regression of the linearized form of eq. (3) (diamonds) and eq. (4) (squares). For nanoparticle acronym and composition please refer to experimental section

3.6 *In vivo* behavioural test

Behavioural tests were conducted in rats to study the efficacy of SLN/P80-URB597 to affect brain function and behaviour. Indeed, it has previously been shown that the anandamide

hydrolysis inhibitor URB597, dissolved in PEG400/P80/saline and given by i.p. injection, has prosocial effects in rats: it increases social play (Manduca et al. 2014; Trezza and Vanderschuren 2008a; Trezza and Vanderschuren 2008b) and corrects the social and communicative deficits observed in an animal model of autism spectrum disorders (Servadio et al. 2016). In the present study, the non-invasive i.n. administration route was exploited as alternative to i.p. administration. Indeed, it has been suggested that i.n. administration enables the direct drug transport to the brain through olfactory nerve, by-passing in this way the BBB (Wen 2011).

Fig. 8 shows the effects of SLN/P80 or SLN/P80-URB597, given to rats by i.n. administration, on social play behaviour. The data demonstrate that SLN/P80-URB597 increased social play behaviour in rats, since it enhanced pouncing (A, $t = 3.82$; $p < 0.01$; $df = 9$) and pinning (B, $t = 3$; $p < 0.05$; $df = 9$) frequencies without affecting the total time spent in social exploration (C, $t = 0.14$; $p = \text{n.s.}$; $df = 9$). These data show that SLN/P80-URB597, given by i.n. route, induces behavioural effects comparable to those induced by i.p. injection of URB597 dissolved in PEG400/P80/saline. Indeed, as previously reported, URB597, dissolved in PEG400/P80/saline and administered i.p. at the dose of 0.1 mg/kg, increased social play behaviour in rats, without affecting general social exploration. Thus, the behavioural analysis performed on pinning and pouncing frequencies and on time spent in social exploration of animals treated either with URB597 dissolved in PEG400/P80/saline or plain PEG400/P80/saline gave the following results: pouncing ($t = 3.86$; $p < 0.001$; $df = 20$); pinning ($t = 2.1$; $p < 0.05$; $df = 20$); social exploration ($t = 0.32$; $p = \text{n.s.}$; $df = 20$) (Fig. 1S, supplementary data).

4 Conclusion

The present study demonstrated that lipid nanoparticles can be efficiently employed to solubilize lipophilic molecules and to administer them, avoiding the use of unphysiological solvents or solvent mixtures. Indeed, RP and PRG solubility was increased respectively 4- and 8-fold using lipid nanoparticles instead of PEG400/P80/saline usually employed for *in vivo* preclinical studies. Moreover, SLN allowed to improve 1.5-fold the URB597 solubility with respect to PEG400/P80/saline.

The i.n. administration of SLN/P80-URB597 induced behavioral effects similar to those induced by i.p. administration of URB597 dissolved in PEG400/P80/saline, suggesting that the i.n. route could be proposed as an alternative route of administration to exploit the therapeutic potential of

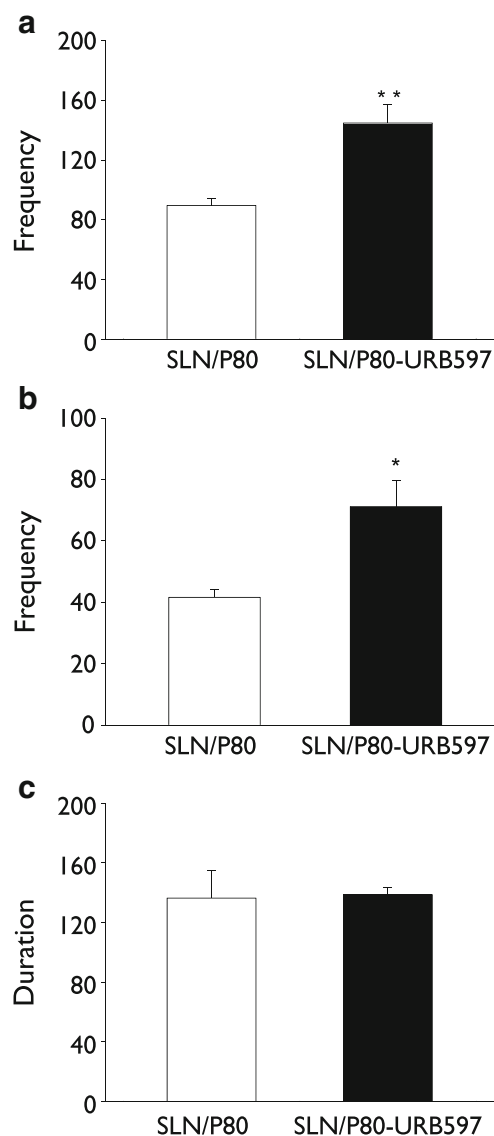


Fig. 8 Social play behavior of rats after intranasal administration of SLN/P80 (white bars) or SLN/P80-URB597 nanoparticles (black bars). **a:** Pouncing. **b:** Pinning. **c:** Social exploration

anandamide hydrolysis inhibitors in social dysfunctions, such as autism.

Acknowledgements This work was funded by "FIRB 2010. Fondo per gli Investimenti della Ricerca di Base" from the Ministry of the University and Research of Italy (code RBFR10XKHS).

References

- E.J.M. Achterberg, V. Trezza, L.J.M.J. Vanderschuren, Glucocorticoid receptor antagonism disrupts reconsolidation of social reward-related memories in rats. *Behav. Pharmacol.* **2**(216–225) (2014)
- A. Ambruosi, H. Yamamoto, J. Kreuter, Body distribution of polysorbate-80 and doxorubicin-loaded [14C]poly(butyl cyanoacrylate) nanoparticles after i.v. administration in rats. *J. Drug Target* **13**, 535–542 (2005)

- M.L. Amin, P-glycoprotein inhibition for optimal drug delivery. *Drug Target Insights* **7**, 27–34 (2013)
- W.A. Banks, Characteristics of compounds that cross the blood-brain barrier. *BMC Neurology* **9**(Suppl 1), S3 (2009)
- R. Bompreszi, Dimethyl fumarate in the treatment of relapsing–remitting multiple sclerosis: An overview. *Ther. Adv. Neurol. Disord.* **8**, 20–30 (2015)
- Cosmetic Ingredient Review Expert Panel, Final report of the safety assessment of alcohol denat., including SD Alcohol 3-A, SD Alcohol 30, SD Alcohol 39, SD Alcohol 39-B, SD Alcohol 39-C, SD Alcohol 40, SD Alcohol 40-B, and SD Alcohol 40-C, and the Denaturants, Quassin, Brucine Sulfate/Brucine, and Denatonium Benzoate. *Int. J. Toxicol* **27**, 1–43 (2008)
- E. Esposito, M. Fantin, M. Marti, M. Drechsler, L. Paccamiccio, P. Mariani, E. Sivieri, F. Lain, E. Menegatti, M. Morari, R. Cortesi, Solid lipid nanoparticles as delivery systems for bromocriptine. *Pharm. Res.* **25**, 1521–1530 (2008)
- E. Esposito, P. Mariani, L. Ravani, C. Contado, M. Volta, Simone Bido, M. Drechsler, S. Mazzoni, E. Menegatti, M. Morari, R. Cortesi, Nanoparticulate lipid dispersions for bromocriptine delivery: Characterization and *in vivo* study. *Eur. J. Pharm. Biopharm.* **80**, 306–314 (2012)
- E. Esposito, L. Ravani, M. Drechsler, P. Mariani, C. Contado, J. Ruokolainen, P. Ratano, P. Campolongo, V. Trezza, C. Nastruzzi, R. Cortesi, Cannabinoid antagonist in nanostructured lipid carriers (NLC): Design, characterization and *in vivo* study. *Mat. Sci. Eng. C* **48**, 328–336 (2015)
- E. Esposito, M. Drechsler, R. Cortesi, C. Nastruzzi, Encapsulation of cannabinoid drugs in nanostructured lipid carriers. *Eur. J. Pharm. Biopharm.* **102**, 87–91 (2016)
- T.M. Göppert, R.H. Müller, Polysorbate-stabilized solid lipid nanoparticles as colloidal carriers for intravenous targeting of drugs to the brain: Comparison of plasma protein adsorption patterns. *J. Drug Target.* **13**, 179–187 (2005)
- V. Jennings, A.F. Thunemann, S.H. Gohla, Characterisation of a novel solid lipid nanoparticle carrier system based on binary mixtures of liquid and solid lipids. *Int. J. Pharm.* **199**, 167–177 (2000)
- K. Jores, W. Mehnert, M. Drechsler, H. Bunjes, C. Johann, K. Maeder, Investigations on the structure of solid lipid nanoparticles (SLN) and oil-loaded solid lipid nanoparticles by photon correlation spectroscopy, field-flow fractionation and transmission electron microscopy. *J. Control. Release* **95**, 217–227 (2004)
- M.D. Joshi, R.H. Müller, Lipid nanoparticles for parenteral delivery of actives. *Eur. J. Pharm. Biopharm.* **71**, 161–172 (2009)
- Y. Kawabata, K. Wada, M. Nakatani, S. Yamada, S. Onoue, Formulation design for poorly water-soluble drugs based on biopharmaceutics classification system: Basic approaches and practical applications. *Int. J. Pharm.* **420**, 1–10 (2011)
- R.A. Linker, R. Gold, Dimethyl fumarate for treatment of multiple sclerosis: Mechanism of action, effectiveness and side effects. *Curr. Neurol. Neurosci. Rep.* **13**, 394 (2013)
- Y. Liu, J. Qiu, Z. Wang, W. You, L. Wu, C. Ji, G. Chen, Dimethylfumarate alleviates early brain injury and secondary cognitive deficits after experimental subarachnoid hemorrhage via activation of Keap1-Nrf2-ARE system. *J. Neurosurg.* **123**, 915–923 (2015)
- V. Luzzati, H. Delacroix, T. Gulik-Krzywicki, P. Mariani, R. Vargas, The cubic phases of lipids. *Curr. Top. Membr.* **44**, 3–24 (1997)
- M. Maden, Retinoic acid in the development, regeneration and maintenance of the nervous system. *Nat. Rev. Neurosci.* **8**, 755–765 (2007)
- A. Manduca, M. Servadio, P. Campolongo, M. Palmery, L. Trabace, L.J. Vanderschuren, V. Cuomo, V. Trezza, Strain- and context-dependent effects of the anandamide hydrolysis inhibitor URB597 on social behavior in rats. *Eur. Neuropsychopharmacol.* **24**, 1337–1348 (2014)
- A.A. Martinez, M.G. Morgese, A. Pisanu, T. Macheda, M.A. Paquette, A.T. Seillier, Activation of PPAR gamma receptors reduces levodopa-induced dyskinesias in 6-OH DA-lesioned rats. *Neurobiol. Dis.* **74**, 295–304 (2015)
- E. Merisko-Liversidge, G.G. Liversidge, Nanosizing for oral and parenteral drug delivery: A perspective on formulating poorly-water soluble compounds using wet media milling technology. *Adv. Drug Del. Rev.* **63**(427–440) (2011)
- P. Montaguti, E. Melloni, Acute intravenous toxicity of dimethyl sulfoxide, polyethylene glycol 400, dimethylformamide, absolute ethanol, and benzyl alcohol in inbred mouse strains. *Arzneimittelforschung* **44**, 566–570 (1994)
- M. Morena, B. Roozendaal, V. Trezza, P. Ratano, A. Peloso, D. Hauer, P. Atsak, L. Trabace, V. Cuomo, J.L. McGaugh, G. Schelling, P. Campolongo, Endogenous cannabinoid release within prefrontal-limbic pathways affects memory consolidation of emotional training. *Proc. Natl. Acad. Sci. U S A* **111**, 18333–18338 (2014)
- M. Morena, V. De Castro, J.M. Gray, M. Palmery, V. Trezza, B. Roozendaal, Training-associated emotional arousal shapes endocannabinoid modulation of spatial memory retrieval in rats. *J. Neurosci.* **35**, 13962–13974 (2015)
- M.G. Morgese, T. Cassano, S. Gaetani, T. Macheda, L. Laconca, P. Dipasquale, L. Ferraro, T. Antonelli, V. Cuomo, A. Giuffrida, Neurochemical changes in the striatum of dyskinetic rats after administration of the cannabinoid agonist WIN55,212-2. *Neurochem. Int.* **54**, 56–64 (2009)
- H. Mu, R. Holma, A. Müllertz, Lipid-based formulations for oral administration of poorly water-soluble drugs. *Int. J. Pharm.* **453**, 215–224 (2013)
- J. Panksepp, W.W. Beatty, Social deprivation and play in rats. *Behav. Neural Biol.* **30**, 197–206 (1980)
- G.M. Pastino, B. Asgharian, K. Roberts, M.A. Medinsky, J.A. Bond, A comparison of physiologically based pharmacokinetic model predictions and experimental data for inhaled ethanol in male and female B5C3F1 mice, F344 rats and humans. *Toxicol. Appl. Pharmacol.* **145**, 147–157 (1997)
- R. Pecora, Dynamic light scattering measurement of nanometer particles in liquids. *J. Nanopart. Res.* **2**, 123–131 (2000)
- S.M. Pellis, V. Pellis, Play-fighting differs from serious fighting in both target of attack and tactics of fighting in the laboratory rat *Rattus norvegicus*. *Aggress. Behav.* **13**, 227–242 (1987)
- N.A. Peppas, Analysis of Fickian and non-Fickian drug release from polymers. *Pharm. Acta Helv.* **60**, 110–111 (1985)
- D. Piomelli, G. Tarzia, A. Duranti, A. Tontini, M. Mor, T.R. Compton, O. Dasse, E.P. Monaghan, J.A. Parrott, D. Putman, Pharmacological profile of the selective FAAH inhibitor KDS-4103 (URB597). *CNS Drug. Rev.* **12**, 21–38 (2006)
- A.A. Saboor-Yaraghi, M.H. Harirchian, N. Mohammadzadeh Honarvar, S. Bitarafan, M. Abdolahi, F. Siassi, E. Salehi, M.A. Sahraian, M.R. Eshraghian, T. Roostaei, F. Koohdani, The effect of vitamin a supplementation on FoxP3 and TGF- β Gene expression in Avonex-treated multiple sclerosis patients. *J. Mol. Neurosci.* **56**, 608–612 (2015)
- M. Servadio, F. Melancia, A. Manduca, A. di Masi, S. Schiavi, V. Cartocci, V. Pallottini, P. Campolongo, P. Ascenzi, V. Trezza, Targeting anandamide metabolism rescues core and associated autistic-like symptoms in rats prenatally exposed to valproic acid. *Transl. Psychiatry* **6**(e902) (2016)
- S. Shah, S. Maddineni, J. Lu, M.A. Repka, Melt extrusion with poorly soluble drugs. *Int. J. Pharm.* **453**, 233–252 (2013)
- J. Siepmann, F. Siepmann, Mathematical modeling of drug delivery. *Int. J. Pharm.* **364**, 328–343 (2008)
- V. Trezza, L.J. Vanderschuren, Bidirectional cannabinoid modulation of social behavior in adolescent rats. *Psychopharmacology* **197**, 217–227 (2008a)

- V. Trezza, L.J. Vanderschuren, Cannabinoid and opioid modulation of social play behavior in adolescent rats: Differential behavioral mechanisms. *Eur. Neuropsychopharmacol.* **18**, 519–530 (2008b)
- V. Trezza, R. Damsteegt, A. Manduca, S. Petrosino, L.W. Van Kerkhof, R.J. Pasterkamp, Y. Zhou, P. Campolongo, V. Cuomo, V. Di Marzo, L.J. Vanderschuren, Endocannabinoids in amygdala and nucleus accumbens mediate social play reward in adolescent rats. *J. Neurosci.* **32**, 14899–14908 (2012)
- L.J. Vanderschuren, B.M. Spruijt, T. Hol, R.J. Niesink, J.M. Van Ree, Sequential analysis of social play behavior in juvenile rats: Effects of morphine. *Behav. Brain Res.* **72**, 89–95 (1995)
- C.L.-N. Vo, C. Park, B.-J. Lee, Current trends and future perspectives of solid dispersions containing poorly water-soluble drugs. *Eur. J. Pharm. Biopharm.* **85**, 799–813 (2013)
- K.M. Webster, D.K. Wright, M. Sun, B.D. Semple, E. Ozturk, D.G. Stein, T.J. O'Brien, S.R. Shultz, Progesterone treatment reduces neuroinflammation, oxidative stress and brain damage and improves long-term outcomes in a rat model of repeated mild traumatic brain injury. *J. Neuroinflamm.* **12**, 238 (2015)
- M.M. Wen, Olfactory targeting through intranasal delivery of biopharmaceutical drugs to the brain: current development. *Discov. Med* **11**, 497–503 (2011)